Phase detection of chaos

Rosangela Follmann* and Elbert E. N. Macau
Associate Laboratory for Computing and Applied Mathematics—LAC, Brazilian National Institute for Space Research—INPE, Brazil

Epaminondas Rosa Jr.
Department of Physics, Illinois State University, Illinois 61790, USA

(Received 14 July 2010; revised manuscript received 3 December 2010; published 21 January 2011)

A technique, first introduced in the context of pseudoperiodic sound waves, is here applied to the problem of detecting the phase of phase coherent and also phase noncoherent chaotic oscillators. The approach is based on finding sinusoidal fits to segments of the signal, therefore obtaining, for each segment, an appropriate frequency from which a phase can be derived. Central to the method is a judicious choice for the size of a sliding window and for the frequency range, as well as for the window advancing step. The approach is robust against moderate noise levels and three cases are presented for demonstrating the applicability of the method.

DOI: 10.1103/PhysRevE.83.016209 PACS number(s): 05.45.Xt, 05.45.Gg

I. INTRODUCTION

Synchronization is everywhere. From simple devices like pendulum clocks to more complex processes like Parkinson's disease it is not uncommon to find systems oscillating in unison [1–4]. Understandably, the amount of recent literature on the subject is enormous, including the various types of synchronization (complete, incomplete, phase, lag, generalized) [5–11]. Among them, phase synchronization is of particular interest due to its wide range of applications. This is the type of synchronization where the synchronized systems maintain no correlation between their amplitudes, but keep their phases in step with each other. A number of techniques for detecting phase synchronism have been developed, including straightforward angle measurements on the attractor [12], Hilbert transform [7], Poincaré surface of section [8], curvature and recurrence plots [13,14], localized sets [15], short-time Fourier transform [16], and wavelets [17]. All these techniques are directly applicable to oscillators with coherent attractors for which the trajectory goes around a fixed center of rotation, and the phase can be defined as the increasing angle between the radius of the trajectory and an arbitrary fixed reference axis. This is not the case for phase noncoherent attractors, for which detecting phase synchrony poses a more challenging task since they do not have a well-defined center of rotation. For this situation, so far there is no general methodology that can be applied with efficacy, in particular if the data series came from an experiment [18].

The method we propose here, introduced in the context of pseudoperiodic sound waves [19], applies to both phase coherent and phase noncoherent oscillators. It is based on a least-square spectral analysis to fit sinusoidal functions to segments of oscillating signals. The technique does not require following the trajectory on the attractor, works well over a wide range of adjustable parameters, is of easy implementation, and is particularly appealing for experimental settings with single signal outputs since there is no need of attractor reconstruction. It consists of an algorithm for estimation of a fundamental frequency for short segments, or windows, along the whole extension of the signal, and it operates by minimizing the square error of fitting a sinusoidal function to the series segment. The use of this least-square parameter estimation makes the method intrinsically resilient to the presence of noise.

II. PHASE ESTIMATION BY MEANS OF FREQUENCY

Consider an oscillating time series $y(t)$ from which we select a segment with K points $y(t_k)$, where time t_k, $k = 1, \ldots, K$, is equally spaced, and write

$$\hat{y}(t_k) = \beta_1 \sin(\omega\, t_k) + \beta_2 \cos(\omega\, t_k) + \beta_3 \tag{1}$$

as an approximation to $y(t_k)$, where ω is the frequency of the sinusoid and β_1, β_2, and β_3 are parameters to be estimated. In matrix form we then write

$$\hat{\mathbf{Y}} = \begin{bmatrix} \sin(\omega\, t_1) & \cos(\omega\, t_1) & 1 \\ \sin(\omega\, t_2) & \cos(\omega\, t_2) & 1 \\ \vdots & \vdots & \vdots \\ \sin(\omega\, t_K) & \cos(\omega\, t_K) & 1 \end{bmatrix} \cdot \begin{bmatrix} \beta_1 \\ \beta_2 \\ \beta_3 \end{bmatrix}. \tag{2}$$

Therefore, $\mathbf{Y} = \mathbf{M}\boldsymbol{\beta} + \boldsymbol{\epsilon}$, where $\boldsymbol{\epsilon}$ is the error of this approximation.

For a given value of ω, the vector parameter $\boldsymbol{\beta}$ is estimated using the least-squared error by minimizing

$$\xi = \sum_{k=1}^{N} \epsilon_k^2 = \boldsymbol{\epsilon}^T \boldsymbol{\epsilon} = (\mathbf{Y} - \mathbf{M}\boldsymbol{\beta})^T (\mathbf{Y} - \mathbf{M}\boldsymbol{\beta}). \tag{3}$$

This yields

$$\boldsymbol{\beta} = [\mathbf{M}^T \mathbf{M}]^{-1} \mathbf{M}^T \mathbf{Y}, \tag{4}$$

which corresponds to the minimum square error.

In order to find the frequency ω, for the appropriate sinusoidal component, we need to evaluate the square error (as a function of ω) that minimizes $\xi(\omega)$. The length of the selected segment plays an important role in this computation and there is no general rule for finding its proper value. Each case needs to be analyzed individually taking into account details like the signal sampling rate and the average number of points per

*rosangela@lac.inpe.br

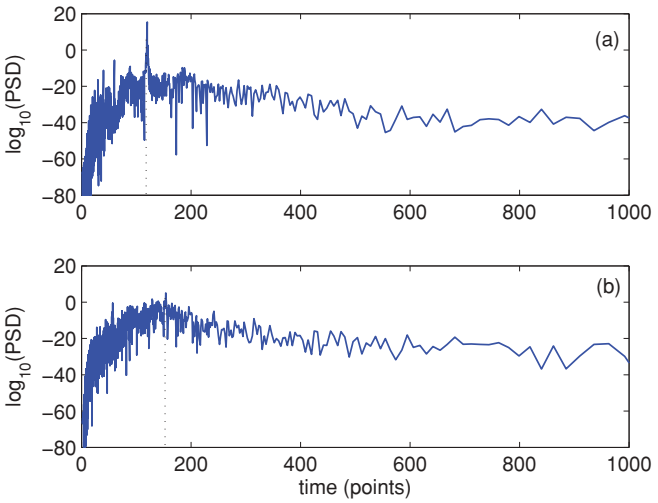

FIG. 1. (Color online) Periodogram of Rössler (a) coherent and (b) noncoherent series. The dotted lines indicate the positions of the corresponding average cycles.

oscillation. However, a simple analysis of the periodogram of the signal can provide an empirical guideline for the average number of points per cycle to be used as reference for the length of the segment. For example, the periodograms for the coherent and noncoherent Rössler systems (the equations are introduced in the next section), as shown in Fig. 1, indicate cycles with (a) 120 points and (b) 150 points, respectively. Numerically we find it suitable, and it makes good sense, to choose a segment length larger than the average cycle obtained from the periodogram. This is illustrated in Fig. 2 where we use three different segment lengths to compute the error function $\xi(\omega)$. The number of points per segment is 280 for plot (a), 320 for plot (b), and 640 for plot (c), coherent, and likewise for plots (d), (e), and (f), noncoherent. Notice the flexibility of the proposed method regarding the choice for the length of the segment. All the cases in this example show the valley point (minimum ξ) at an ω value around 1.0, not atypical for the Rössler system. The chosen frequency value in each case is

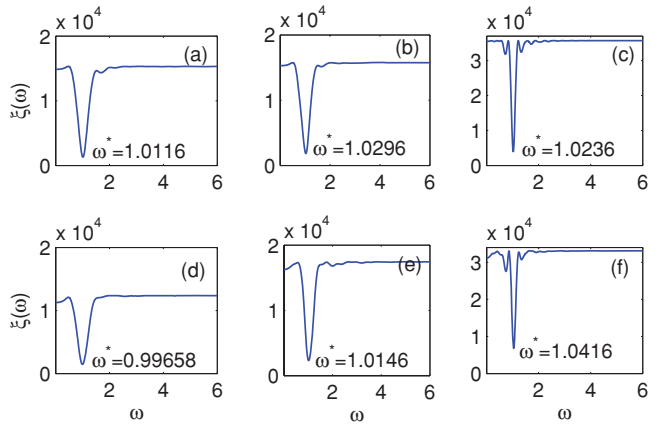

FIG. 2. (Color online) Error function $\xi(\omega)$ for 1000 values of $\omega \in [0:6]$. (a) 280-point, (b) 320-point, and (c) 640-point sample segment of Rössler coherent trajectory; (d) 280-point, (e) 320-point, and (f) 640-point sample segment of Rössler noncoherent trajectory. ω^* expresses the estimated frequency value.

expressed by ω^* which is the frequency to be used to obtain the phase ϕ for that particular segment, taking into account that $d\phi/dt = \omega$.

The whole extend of the signal needs to be scanned through with a sliding window allowing for some overlapping as it advances. The size of the window is the same as that of the segment, given by $y(t_{k+n.S})$, $n = 0, \ldots, N$ and $k = 1, \ldots, K$, where N is the total number of points of the series, K is the length of the selected segment (window size), and S is the size of the step for the advancing window. A frequency will be extracted for each advance of the window, and the corresponding phase will be computed by applying a cumulative numerical integration using the trapezoidal method over all estimated frequencies.

The technique we propose here then requires (i) selecting a segment length containing at least two full signal cycles; (ii) selecting a small range of frequencies, from an initially wide range, using the minimum error function analysis; (iii) the step for consecutive window advances (all examples presented here use $S = 1$); and (iv) using the trapezoidal integration method for obtaining the phases. The sequence of these four points summarizes the method from here on referred to as PEMF, an acronym for phase estimation by means of frequency.

III. PHASE SYNCHRONIZATION DETECTION

We now implement the PEMF method using coupled chaotic oscillators in order to identify their phase synchronous regimes. The method obtains the phases ϕ_1 and ϕ_2 of the oscillators, and then the locking condition $\Delta\phi(t) \equiv |n\phi_1(t) - m\phi_2(t)| \leqslant 2\pi$ is tested. Here we consider the $n = m = 1$ case and demonstrate the applicability of the proposed method to four different setups. In the first three setups we compare the PEMF method with other methods, and in the fourth setup we apply the method to a forced plasma experimental time series.

Among the other methods mentioned in the Introduction, the three more closely related to our PEMF method are the short-time Fourier transform [16], the Hilbert transform [7], and wavelets [17] (see Ref. [16] for a comparative study of the three approaches). The wavelets technique has been applied to noncoherent oscillations [17], but we are not aware of this being the case for the short-time Fourier and Hilbert transforms. Therefore we here choose to compare our approach in both coherent and noncoherent cases first with other more direct measurements and also with the continuous wavelet method with the Morlet wavelet as the mother function [20].

A. Coherent Rössler system

In this first case we use two coupled Rössler oscillators [12,21],

$$\begin{aligned} \dot{x}_{1,2} &= -\omega_{1,2} y_{1,2} - z_{1,2} + \eta(x_{2,1} - x_{1,2}), \\ \dot{y}_{1,2} &= -\omega_{1,2} x_{1,2} + a y_{1,2}, \\ \dot{z}_{1,2} &= 0.1 + z_{1,2}(x_{1,2} - 8.5), \end{aligned} \tag{5}$$

where a governs the topology of the attractor, η is the coupling strength, $\omega_1 = 0.98$ and $\omega_2 = 1.02$ establish the mismatch in the natural frequencies of the two oscillators, and integration step $h = 0.05$. For $a = 0.16$ the attractor is phase coherent

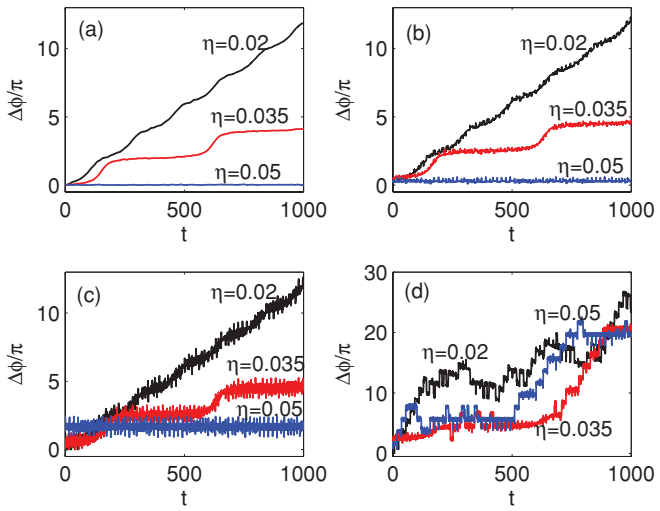

FIG. 3. (Color online) Time evolution of the phase difference of the Rössler oscillators in a phase coherent regime ($a = 0.16$) for three different intensities of coupling, as indicated, for (a) the PEMF method, (b) the arctangent method, (c) the wavelet method with time scale $s = 5.4$, and (d) the wavelet method with time scale $s = 5.5$.

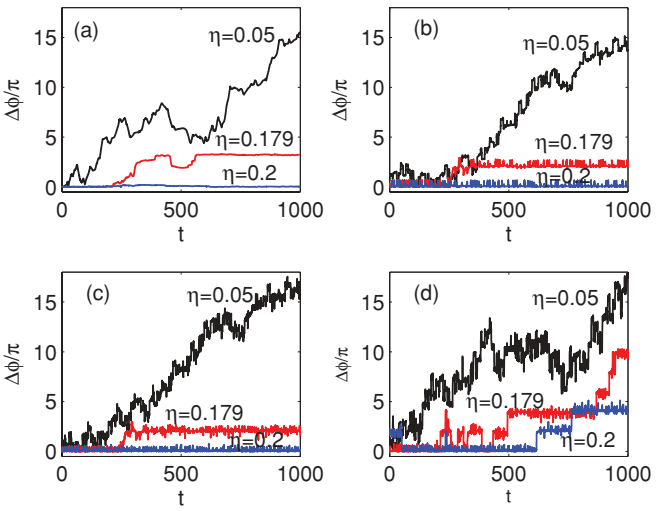

FIG. 4. (Color online) Time evolution of the phase difference of Rössler oscillators in a phase noncoherent regime ($a = 0.2925$) for three different intensities of coupling, as indicated, for (a) the PEMF method, (b) the curvature method, (c) the wavelet method with time scale $s = 5.4$, and (d) the wavelet method with time scale $s = 5.5$.

and the results of applying the PEMF method for three different values of the coupling η are shown in Fig. 3(a). This figure displays the phase differences between the two coupled oscillators, indicating clearly the tendency to synchronization as η increases. The phases are estimated by using a sliding window of length $K = 540$ points containing about four oscillations of the Rössler x component. For the frequencies ω we use 200 equally spaced values between 0.6 and 1.4.

In order to validate the PEMF method we check our results against the results obtained using the standard phase definition $\phi(t) = \arctan(y/x)$ [7] and applying the continuous wavelet transform [20]. We compute the phases differences for the same Rössler equations with the same three coupling parameter values as those used in the PEMF. Figure 3(b) shows the results using the arctangent method, and the results using wavelet analysis, with time scale $s = 5.4$, are shown in Fig. 3(c), demonstrating the agreement between the three methods, except perhaps for smoother lines representing phases differences in the PEMF method. Basically, the three approaches show that, for stronger coupling ($\eta = 0.05$), the two Rössler oscillators have their phases in step with each other, therefore in synchrony, keeping the phase difference $\Delta\phi$ between them small and less than 2π. For a weaker coupling ($\eta = 0.035$), the synchrony breaks with steps of 2π in $\Delta\phi$, and more so with an even weaker coupling ($\eta = 0.020$). As is the case for the PEMF method, the wavelet method does not require the finding of a center of rotation for the attractor. However, as opposed to the PEMF method, the wavelet method is very sensitive to time scale parameter changes. For example, using $s = 5.5$ instead of $s = 5.4$ yields completely altered results as illustrated in Fig. 3(d).

B. Noncoherent Rössler system

For the phase noncoherent system (parameter $a = 0.2925$), when the Rössler attractor goes into the funnel regime with no well-defined center of rotation in the attractor [12], the PEMF method is applicable in the same manner as done in the phase coherent situation, except that the lack of a well-defined center of rotation for the attractor makes the PEMF method more sensitive to the window size. The larger variability of the phase noncoherent Rössler x component in fact requires a smaller sliding window ($K = 280$) for the same range of the frequency ω used before ([0.6 : 1.4]). The PEMF method results for three different coupling values are depicted in Fig. 4(a). As the arctan phase definition used above for coherent systems is rendered useless for noncoherent signals, we resort to the curvature approach to define the phase $\phi = \arctan(\dot{y}/\dot{x})$ [14,22] and compute the phases differences for the same system. The results are shown in Fig. 4(b), demonstrating consistency with the PEMF method. Figures 4(c)–4(d) show the results using the wavelet transform with $s = 5.4$ and $s = 5.5$, respectively. As in the coherent case, the wavelet transform results are very sensitive to the time scale parameter s with a small range of usability, $s \in [5.1 : 5.4]$. However, the PEMF method possesses a wide range of window length choices as we will show next.

We now discuss the window size relation to the phase, as mentioned previously in the case of noncoherent attractors. In order to demonstrate the effect of different window sizes in both coherent and noncoherent cases, we plot in Fig. 5 the variance of the phase difference between two phase synchronized Rössler systems versus the window size. All phases here are computed using the PEMF method. In the coherent case [Fig. 5(a)] there is a noticeable wide range of windows yielding small variances, indicating, in particular, that a window size in the range [160 : 1000] would be fine. However, the range for the window size in the noncoherent case is smaller, as shown in Fig. 5(b). It is now restricted between 180 and 670 points. These numbers are compatible with the values discussed in Sec. II for the length of the segment.

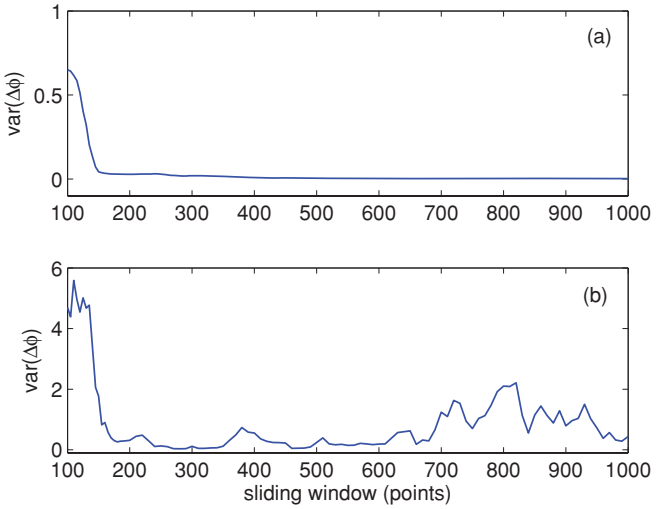

FIG. 5. (Color online) Variance of the phase difference as a function of the sliding window size. (a) Rössler oscillators with $a = 0.16$ (coherent) and coupling strength $\eta = 0.05$; (b) phase noncoherent regime ($a = 0.2925$) and coupling strength $\eta = 0.2$.

The influence of noise on the performance of the PEMF method is now investigated. Adding noise to the components of the coherent Rössler system studied previously, the signals become $\tilde{x}_{1,2}(t) = x_{1,2}(t) + \alpha\sigma_{1,2}\vartheta_{1,2}(t)$, where $\vartheta_{1,2}(t)$ is an independent uniformly distributed noise with zero mean and standard deviation equal to 1. $\sigma_{1,2}$ are the standard deviations of components x_1 and x_2, respectively, and α is the noise level. We pick the coupling strength $\eta = 0.05$ with noise level $\alpha = 0.8$. The results obtained with the PEMF method using the same window size and frequency range as before are shown in Fig. 6(a) without noise and Fig. 6(b) with noise. Notice the modest increase in the phase difference between the noisy signals compared with the clean signals, clearly indicating that the method is robust against moderate noise levels. This is because our method is based on a least-square parameter estimation, which per se is very resilient to the presence of noise.

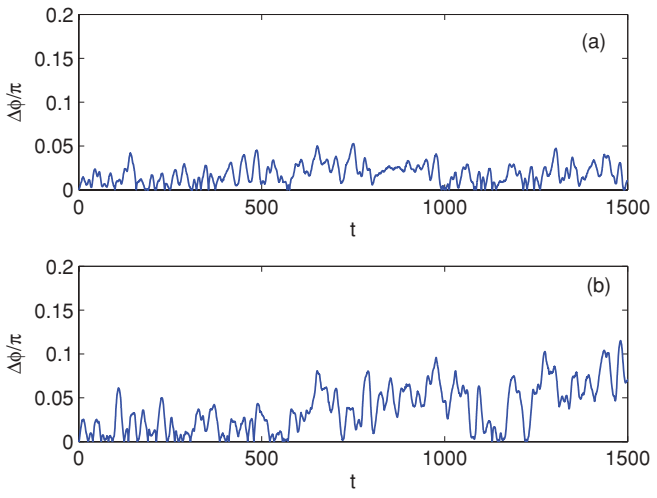

FIG. 6. (Color online) Phase difference of two coupled Rössler oscillators in the phase synchronization state ($\eta = 0.05$). (a) Without noise; (b) with 80% Gaussian observational noise.

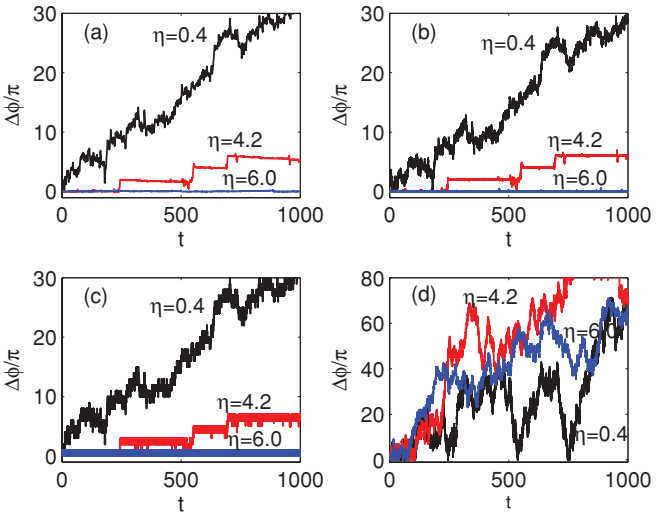

FIG. 7. (Color online) Time evolution of the phase difference of two coupled Lorenz systems for three different coupling values: (a) PEMF method, (b) arctangent on the projection of the attractor, (c) wavelet method with $s = 1.0$, and (d) wavelet method with $s = 2.0$.

C. Lorenz system

The well-known Lorenz attractor [23] is another case of a noncoherent attractor for which finding the right definition of phase can be challenging. The double scroll nature of its attractor in fact precludes coupled Lorenz systems from experiencing phase synchronization [24,25]. Nevertheless, the PEMF method still produces good results, as shown in Fig. 7, obtained from the two coupled Lorenz systems,

$$\begin{aligned} \dot{x}_{1,2} &= 10(y_{1,2} - x_{1,2}) + \eta(x_{2,1} - x_{1,2}), \\ \dot{y}_{1,2} &= 28x_{1,2}z_{1,2} - x_{1,2} - y_{1,2}, \\ \dot{z}_{1,2} &= \omega_{1,2}\left(x_{1,2}y_{1,2} - \tfrac{8}{3}z_{1,2}\right), \end{aligned} \tag{6}$$

where $\omega_1 = 0.9831$ and $\omega_2 = 1.018$ introduce a small mismatch between the two oscillators, η is the coupling strength, and integration step $h = 0.01$. The adequate window length in this case is $K = 130$ and for the frequency range we use 800 equally spaced values between 6 and 12.

For the sake of comparison, we take advantage of the evident symmetry (x, y) to $(-x,-y)$ in the Lorenz equations,

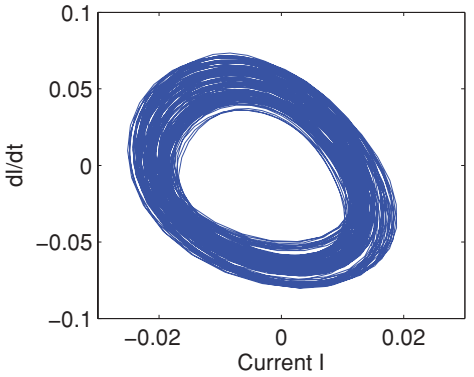

FIG. 8. (Color online) Projection of the plasma attractor in Cartesian coordinates.

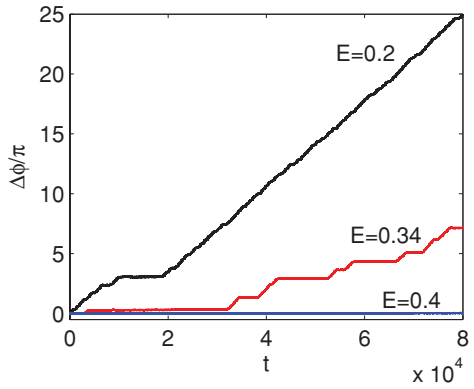

FIG. 9. (Color online) Time evolution of the phase difference of the experimental data for three different forcing amplitudes: $E = 0.2$ V, $E = 0.34$ V, and $E = 0.4$ V.

make a projection of the attractor on the (u,z) plane, where $u = \sqrt{x^2 + y^2}$ [8], and define the phase using the angle $\phi = \arctan\left(\frac{z(t)-z_0}{u(t)-u_0}\right)$. In this equation $u_0 = 12$ and $z_0 = 27$ are introduced for translating the axes of reference to the center of the attractor. In Fig. 7 we show the phase differences for the two coupled systems for three different coupling values using the (a) PEMF method on the z component, using the (b) arctangent method on the projection of the attractor, and using the wavelet approach on the z component with (c) $s = 1$ and with (d) $s = 2$. Notice the consistency of the results obtained using the three methods. The PEMF method uses the time series straightforwardly as it comes and does not require initial data manipulation.

D. Plasma experimental data

In order to illustrate the applicability of the PEMF method to experimental data we use the data of phase synchronization of a chaotic plasma discharge tube subject to the action of a periodic wave generator. The experimental setup and other details can be found in Ref. [26]. We use a signal output from a plasma discharge tube subject to a voltage of 850 V. The power spectrum of the signal is broad with a predominant frequency of 6960 Hz and with the largest Lyapunov exponent positive, indicating the plasma's chaotic character. Figure 8 shows the reconstructed attractor obtained from the acquired time series.

The phases are estimated by using a sliding window of length $K = 500$ containing about four oscillations and the frequencies used correspond to 500 values between 6660 and 7160 Hz. The results are shown in Fig. 9 for three different intensities of the forcing. When the plasma system is paced with a sine wave with a frequency of 6960 Hz and an amplitude of 0.2 V, we can observe the increase of phase difference over time showing no phase synchronization, except for short-lived plateaus. When the plasma system is paced with a little stronger amplitude of 0.34 V, the evolution of phase difference presents larger plateaus characterizing time intervals of phase synchronization. When the amplitude of the sine wave is increased to 0.4 V we see clearly that the phase difference stops increasing and oscillates around a constant value, indicating phase synchronization for the whole length of the time series.

IV. CONCLUSION

The PEMF method proposed here consists of finding the phase of oscillating signals by obtaining the best sinusoidal fit for selected segments of the oscillating time series. There is no need of attractor projection or reconstruction, which in fact is a major advantage of the method. It is flexible and in principle is applicable to any time series suitable for sinusoidal fittings, as demonstrated through the preceding examples. Care must be taken with the size of the sliding window as well as with the range of the frequencies as there are no standard numbers associated with them. Comparison between the PEMF method and other approaches for finding the phase of oscillating signals demonstrates the efficacy of the method. As shown in Sec. III, the PEMF method yields results that are consistent with the arctangent and wavelet methods in both phase coherent and noncoherent cases. However the arctangent method requires an attractor projection with a well-defined center of rotation that is not needed for the PEMF method. The wavelet method does not require attractors with a well-defined center of rotation, but it is very sensitive to changes in the time scale parameter. It produces altered results for the phase difference in the case of s outside the small range between 5.1 and 5.4, in both coherent and noncoherent cases. This is shown in Figs. 3(d) and 4(d), respectively. The PEMF method, in addition to not involving derivatives or attractor reconstruction, works well in a wide range of the sliding window parameter, which provides a considerable level of flexibility to our approach. It expands on the fundamental frequency estimation technique [19] for appropriate applicability to both phase coherent and especially phase noncoherent systems. The method is particularly suitable for experimental data, is of relatively easy implementation, and is robust against moderate noise levels.

ACKNOWLEDGMENTS

This work is supported by the São Paulo Research Foundation–FAPESP, Grant No. 07/05581-0, and also by CNPq.

[1] C. Huygens, *Horologium Oscillatorium* (Apud F. Muguet, Parisiis, 1673).
[2] S. H. Strogatz and I. Stewart, Sci. Am. **269**, 68 (1993).
[3] C. Schäfer, M. G. Rosenblum, A. S. Pikovsky, and J. Kurths, Nature (London) **392**, 239 (1998).
[4] C. Park, R. M. Worth, and L. L. Rubchinsky, J. Neurophysiol. **103**, 2707 (2010).
[5] T. Yamada and H. Fujisaka, Prog. Theor. Phys. **72**, 885 (1984).
[6] L. M. Pecora and T. L. Carroll, Phys. Rev. Lett. **64**, 821 (1990).
[7] M. G. Rosenblum, A. S. Pikovsky, and J. Kurths, Phys. Rev. Lett. **76**, 1804 (1996).
[8] A. S. Pikovsky, M. G. Rosenblum, G. V. Osipov, and J. Kurths, Physica D **104**, 219 (1997).

[9] T. Yalcinkaya and Y.-C. Lai, Phys. Rev. Lett. **79**, 3885 (1997).
[10] E. Rosa, Jr., E. Ott, and M. H. Hess, Phys. Rev. Lett. **80**, 1642 (1998).
[11] S. Boccaletti, J. Kurths, G. Osipov, D. Valladares, and C. Zhou, Phys. Rep. **366**, 1 (2002).
[12] E. F. Stone, Phys. Lett. A **163**, 367 (1992).
[13] M. C. Romano, M. Thiel, J. Kurths, I. Z. Kiss, and J. L. Hudson, Europhys. Lett. **71**, 466 (2005).
[14] J. Kurths, M. C. Romano, M. Thiel, G. V. Osipov, M. V. Ivanchenko, I. Z. Kiss, and J. L. Hudson, Nonlinear Dyn. **44**, 135 (2006).
[15] T. Pereira, M. S. Baptista, and J. Kurths, Phys. Rev. E **75**, 026216 (2007).
[16] A. Bruns, J. Neurosci. Methods **137**, 321 (2004).
[17] A. E. Hramov and A. A. Koronovskii, Physica D: Nonlinear Phenomena **206**, 252 (2005).
[18] R. Follmann, E. E. Macau, and E. Rosa, Jr., Phys. Lett. A **373**, 2146 (2009).
[19] A. Choi, IEEE Trans. Speech Audio Process. **5**, 201 (1997).
[20] A continuous set of phases $\phi_s(t)$ corresponding to the time scales s of the chaotic signal is determined using a continuous wavelet transform $W(s,t_0) = W(s,t_0)e^{j\phi_s}$. The mother wavelet used is the Morlet wavelet $\Psi_0(\alpha) = (1/\sqrt[4]{\pi})\exp(j\omega_0\alpha)\exp(-\alpha^2/2)$. The wavelet parameter $\omega_0 = 2\pi$ ensures the relation $s \cong 1/f$ between the time scale s and the frequency f of the Fourier transform.
[21] O. E. Rössler, Phys. Lett. A **57**, 397 (1976).
[22] J. Y. Chen, K. W. Wong, and J. W. Shuai, Phys. Lett. A **285**, 312 (2001).
[23] E. N. Lorenz, J. Atmos. Sci. **20**, 130 (1963).
[24] E.-H. Park, M. A. Zaks, and J. Kurths, Phys. Rev. E **60**, 6627 (1999).
[25] Z. Liu, Y.-C. Lai, and M. A. Matías, Phys. Rev. E **67**, 045203 (2003).
[26] C. M. Ticos, E. Rosa, W. P. Pardo, J. A. Walkenstein, and M. Monti, Phys. Rev. Lett. **85**, 2929 (2000).